HHS Public Access

Author manuscript

Neuron. Author manuscript; available in PMC 2017 May 18.

Published in final edited form as:

Neuron. 2016 May 18; 90(4): 824–838. doi:10.1016/j.neuron.2016.04.040.

Enhanced GABA transmission drives bradykinesia following loss of dopamine D2 receptor signaling

Julia C. Lemos[1], **Danielle M. Friend**[2], **Alanna R. Kaplan**[1], **Jung Hoon Shin**[1], **Marcelo Rubinstein**[3], **Alexxai V. Kravitz**[2], and **Veronica A. Alvarez**[1]

[1]National Institute on Alcohol Abuse and Alcoholism, NIH, Bethesda, MD 20892

[2]National Institute of Diabetes and Digestive and Kidney Diseases, NIH, Bethesda, MD 20892

[3]Instituto de Investigaciones en Ingeniería Genética y Biología Molecular, CONICET

[4]FCEN, Universidad de Buenos Aires, Argentina

Summary

Bradykinesia is a prominent phenotype of Parkinson's disease, depression, and other neurological conditions. Disruption of dopamine transmission plays an important role but progress in understanding the exact mechanisms driving slowness of movement has been impeded due to the heterogeneity of DA receptor distribution on multiple cell types within the striatum. Here we show that selective deletion of DA D2 receptors (D2Rs) from indirect-pathway medium spiny neurons (iMSNs) is sufficient to impair locomotor activity, phenocopying DA depletion models of Parkinson's disease, despite this mouse model having intact DA transmission. There was a robust enhancement of GABAergic transmission and a reduction of *in vivo* firing in striatal and pallidal neurons. Mimicking D2R signaling in iMSNs with Gi-DREADDs restored the level of tonic GABAergic transmission and rescued the motor deficit. These findings indicate that DA, through D2R activation in iMSNs, regulates motor output by constraining the strength of GABAergic transmission.

Introduction

Dopamine (DA) depletion, caused by pharmacological agents or genetic models of DA neuron degeneration, produces a pronounced motor deficit that closely resembles the motor symptoms characteristic of Parkinson's disease (Bergman and Deuschl, 2002; Deumens et al., 2002; Lovinger, 2010; Palmiter, 2008; Schultz, 1982; Surmeier et al., 2014). However, this basic research has struggled to accurately and consistently relate the motor deficits produced by dopamine depletion to specific changes in striatal neuronal activity and circuit

Correspondence to be sent to Veronica A. Alvarez at ; Email: alvarezva@mail.nih.gov

Author Contributions: Conceptualization: V.A.A, A.V.K, J.CL, M.R. and A.R.K. Methodology: M.R., V.A.A., A.V.K. and J.C.L. Investigation, Validation and Analysis: J.C.L., D.F.M., A.R.K, J.H.S. Writing – Original Draft: J.C.L and V.A.A Funding: V.A.A., A.V.K., M.R. and J.C.L. Resources: V.A.A., A.V.K and M.R. Supervision: V.A.A. and A.V.K.

function. This is owing, in large part, to technical limitations such as the experimental variability inherent to 6-OHDA lesions (Deumens et al., 2002; Vandeputte et al., 2010) in addition to the biological complexity such as the heterogeneity of DA receptor expression within the basal ganglia (Surmeier et al., 2011).

DA D2 receptors (D2Rs) are critical to motor output because global deletion of D2Rs leads to similar motor deficits as those seen after dopamine depletion (Baik et al., 1995; Kelly et al., 1998; Rubinstein et al., 1990). However, in the striatum alone, D2Rs are expressed on at least five different types of neurons: indirect-pathway MSNs (iMSNs), cholinergic interneurons, a subset of GABA interneurons, and on afferents to the striatum from dopamine and prefrontal cortex neurons (Bamford et al., 2004; Bello et al., 2011; Centonze et al., 2003; Maurice et al., 2004; Surmeier et al., 2011). It is unclear whether ubiquitous activation of all these striatal D2Rs or selective activation of a subset of D2Rs is responsible for generating the motor deficits of DA depletion models. Furthermore, it is unknown whether D2Rs expressed in the cortex and other non-striatal regions that receive projections from midbrain DA neurons also contribute to this motor phenotype. In this study, we generated a mouse line with a precise genetic manipulation that allows for reliable titration of the levels of D2Rs on iMSNs by crossing conditional *Drd2*$^{loxP/loxP}$ mice with mice expressing Cre recombinase selectivity in striatal iMSNs (*Adora2A-Cre*$^{+/-}$). This mouse line, referred to as iMSN-Drd2KO, exhibits bradykinesia while showing normal DA release properties, indicating that downregulation of D2R function in iMSNs is sufficient to recapitulate the motor impairments of DA depletion models.

Based on the “go-no go” model of basal ganglia function, direct-pathway MSNs (dMSNs) and iMSNs exert opposite effects on motor output where increased activity of dMSNs facilitates movement and increased activity of iMSNs suppresses movement (Albin et al., 1989; DeLong, 1972; Delong et al., 1984; Gerfen and Surmeier, 2011). Indeed, manipulations of dMSN and iMSN activity have provided strong support for this model (Bateup et al., 2010; Durieux et al., 2009; Kravitz et al., 2010). Furthermore, the model posits that DA in the striatum enhances locomotion mainly via activation of $G_{s/olf}$-coupled DA D1Rs expressed by direct-pathway MSNs (dMSNs) and activation of $G_{i/o}$-coupled D2Rs expressed by iMSNs (Durieux et al., 2012). This model is the basis for one of the current hypotheses of Parkinson’s disease, which postulates that decreased activity of dMSNs and increased activity of iMSNs, resulting from a lack of D1R and D2R activation respectively, is responsible for the motor impairment. Several studies report enhanced *in vivo* somatic firing rate after 6-OHDA lesion, although this finding has been inconsistent across studies (Chan et al., 2012; Chang et al., 2006; Cho et al., 2002; Costa et al., 2006; Hull et al., 1974; Kish et al., 1999). It is then still unclear how striatal circuit activity changes during the motor impairment and whether these changes are causative or rather homeostatic alterations aimed at compensating for the motor dysfunction. In this study, targeted deletion of D2Rs to striatal iMSNs is performed to parse the specific role of these receptors in controlling neuronal excitability, *in vivo* MSN firing and inhibitory transmission and determine how these cellular changes may relate to the observed motor impairment, one of the main symptoms that defines Parkinson’s disease.

Results

Selective deletion of D2Rs from iMSNs impairs spontaneous locomotion

Mice carrying the conditional *Drd2* allele (*Drd2*$^{loxP/loxP}$) were crossed with BAC transgenic *Adora2A-Cre*$^{+/-}$ mice to generate mice lacking D2Rs selectively in iMSNs throughout the striatum (iMSN-Drd2KO), while preserving other striatal and non-striatal D2Rs. *Adora2A-Cre*$^{+/-}$ transgenic mice provide specific Cre expression in iMSNs (>80% co-expression with met-enkaphalin) with no expression in dMSNs, cholinergic interneurons and midbrain dopamine neurons (Figure S1). There was a pronounced gene-dependent reduction of *Drd2* mRNA in striatal tissue for iMSN-Drd2HET (~40%) and iMSN-Drd2KO mice (>80%) relative to *Drd2*$^{loxP/loxP}$ mice (1W ANOVA: $F_{2, 8} = 83.75$, $p < 0.0001$, n = 3–5 mice) with no reduction in *Drd1* mRNA levels (1W ANOVA, $p = 0.43$; Figure 1a). Locomotor activity in the home cage was reduced by >50% in both iMSN-Drd2HET and iMSN-Drd2KO mice compared to control *Drd2*$^{loxP/loxP}$ littermates (time x genotype interaction, 2WRM ANOVA, $F_{46,759} = 4.635$, $p < 0.0001$, n = 9–14; Figure 1b). When placed in a novel open field chamber, iMSN-Drd2KO mice spent more time immobile (hypokinesia), and were slower when mobile (bradykinesia), contributing to an overall lower distance traveled (85 ± 3% vs. 67 ± 3% immobile for iMSN-Drd2KO and *Drd2*$^{loxP/loxP}$, respectively; speed when mobile (<2 cm/s) = 4.5 cm/s vs. 6 cm/s; 1W ANOVA, $F_{2,59} = 13.9, 29.9$ respectively, $p < 0.0001$, n = 9–28; Figure 1c). In addition, iMSN-Drd2KO mice showed impaired performance on a motor skill task assayed using the rotarod (Figure 1d). iMSN-Drd2HET mice displayed an intermediate phenotype in both assays, (post-hoc tests, $ps < 0.05$ compared to *Drd2*$^{loxP/loxP}$ and iMSN-Drd2KO; n = 9–28; Figure 1c,d), demonstrating haploinsufficiency and the ability of this genetic model to tightly control the expression level of D2Rs and titrate the motor phenotype. These results indicate that reduction of striatal D2R levels specifically in iMSNs is sufficient to reproduce the motor deficits of global D2R knockout mice and dopamine depletion models (Baik et al., 1995; Kelly et al., 1998; Rubinstein et al., 1990) and is opposite to the phenotype following targeted deletion of D2 autoreceptors (Anzalone et al., 2012; Bello et al., 2011).

Pre-clinical studies using 6-OHDA lesions produce motor impairments that are lessened by salient stimuli (Keefe et al., 1989; Rodriguez Diaz et al., 2001), similar to the paradoxical kinesia observed in Parkinson's patients (Bienkiewicz et al., 2013). Interestingly, we also noticed that iMSN-Drd2KO mice showed less motor impairment during the novelty phase of the open field assay (the first minute) and iMSN-Drd2HET displayed similar locomotor response to control *Drd2*$^{loxP/loxP}$ mice during this first minute of open field exposure (post-hoc test, $p = 0.93$, n = 9–24, Figure 1c; S2). These observations suggested that environmental salience could reduce the impact of the motor impairment.

We performed two additional experiments to more directly evaluate the impact of environmental salience. First, we tested whether exposure to a novel object, an appetitive stimulus known to evoke phasic dopamine (Fink and Smith, 1980; Legault and Wise, 2001), would facilitate locomotion in iMSN-Drd2KO mice. When a novel object was introduced in the center of the open field chamber, iMSN-Drd2KO mice spent more time in the object's perimeter and traveled larger distances around the object compared to *Drd2*$^{loxP/loxP}$ mice (t-

test, *ps* = 0.04, n = 20–21). In this context, their speed around the object did not differ from control littermates (t-test, $p = 0.96$, n = 20–21; Figure 1c; S3). Second, we measured motor activity of the same two groups of mice (iMSN-Drd2KO and control $Drd2^{loxP/loxP}$) in two environments that carried different motivational salience: a cylindrical empty chamber and a cylindrical chamber of identical dimensions filled with water. Spontaneous locomotion was measured for 15 min over a two-day period, counterbalanced across animals. In the empty chamber, iMSN-Drd2KO mice displayed a similar motor deficit as seen in the novel open field described above (Figure 1f). In contrast, during forced swim, iMSN-Drd2KO mice did not exhibit significant differences in speed nor distance traveled compared to control $Drd2^{loxP/loxP}$ littermates (t-tests, $p = 0.4$, n = 9–11, Figure 1f). Collectively, the results indicate that the motor activity stimulated by salient stimuli is normal, or even possibly enhanced, in iMSN-Drd2KO compared to control littermates, again replicating the motor phenotype of DA depletion models.

To further evaluate the spatio-temporal dependence of the D2R deletion on the motor impairment, D2R deletion was restricted to the nucleus accumbens (NAc) of adult mice using bilateral stereotaxic injections of AAV viral vectors expressing Cre recombinase in the NAc of adult (>p60) $Drd2^{loxP/loxP}$ mice (Figure 2a,b). This manipulation, while not selective for iMSNs, produced an 80% reduction of *Drd2* mRNA levels in the NAc (Figure 2c) and minimizes possible compensatory changes caused by lack of D2Rs during brain development. Knock-down of D2Rs in the NAc decreased homecage locomotion (time x viral type interaction, 2WRM ANOVA, $F_{23,276} = 1.83$, $p = 0.01$, main effect of viral type: $F_{23,276} = 6.65$, $p = 0.008$, n = 5–9; Figure 2d). Moreover, NAc-*Drd2* knock-down reduced horizontal locomotor activity in a novel locomotor chamber compared to GFP expressing mice (2WRM ANOVA, main effect of viral type, $F_{1,20} = 17.68$, $p = 0.004$, n = 10–12, Figure 2e). The pattern of locomotor activity between naïve $Drd2^{loxP/loxP}$ control mice and $Drd2^{loxP/loxP}$ expressing GFP viral particles was nearly identical (2WRM ANOVA, $F_{11,308} = 0.5$, $p = 0.55$, n = 12–18). Acute knockdown of D2Rs in the NAc completely recapitulated the locomotor deficit observed in iMSN-Drd2KO mice in this particular behavioral assay (2WRM ANOVA, $F_{11,209} = 0.5$ $p = 0.63$, n = 10–11). However, acute knock-down of D2Rs in the NAc did not impair motor skill performance or motor skill learning on a rotarod (2WRM ANOVA, $F_{25,325} = 0.73$, $p = 0.39$, n = 6–9, Figure 2f). These results are consistent with other studies that suggest a regional dissociation between spontaneous locomotion and motor skill learning (Durieux et al., 2012) and are complementary to recent findings showing increased locomotion following D2R overexpression in the NAc (Gallo et al., 2015). Taken together, these results demonstrate that the locomotor deficit does not require absence of D2Rs throughout development. Moreover, it suggests that manipulating dopamine transmission in the NAc alone can alter movement.

Evoked DA release and D2 autoreceptor modulation are intact in iMSN-Drd2KO mice

Fast scan cyclic voltammetry was used to measure DA signals in both the dorsal striatum (DS) and the NAc in brain slices from iMSN-Drd2KO and control $Drd2^{loxP/loxP}$ mice. In the DS, the DA concentrations evoked by 1 pulse stimulation were higher than the NAc and there were no differences between genotypes (2W ANOVA, main effect of region: $F_{1,36} = 10.52$, $p = 0.003$; no region x genotype interaction: $F_{1,36} = 1.3E\text{-}5$, $p = 0.99$, n = 7–14;

Figure 3a,b). Single pulse stimulation evoked the maximal DA concentration transient at 0.5 msec duration in both genotypes, which plateaued with = 10.89, $p < 0.0001$, longer durations (2WRM ANOVA, main effect of stim duration: $F_{5,60}$ Figure 3c). There was no difference between genotypes in the peak DA concentration following 20p stimulation or in the 1p:20p ratio, which was higher in the NAc than in the DS (2W ANOVA, main effect of region, $F_{1,36} = 13.36$, $p = 0.0008$; no region x genotype interaction: $F_{1,36} = 0.1371$, $p = 0.7$, n = 7–14; Figure 3d,e) Sulpiride, a D2-like receptor antagonist, increased DA transients evoked by trains and, as expected the increase was greater in the NAc than in the DS (2WRM ANOVA, main effect of region, $F_{1,12} = 15.13$, $p = 0.002$, Figure 3f,g). Importantly, the effect of sulpiride was similar in both genotypes (region x genotype interaction, 2W ANOVA, $F_{1,25} = 0.33$, $p = 0.53$, n = 5–8, Figure 3f,g) as was the effect of a D2-like agonist, quinpirole at the IC_{50} concentration (0.03μM) or maximal concentration of 1 μM (drug concentration x genotype interaction, 2W ANOVA, $F_{2,24} = 1.47$, $p = 0.25$, n = 4–9, Figure 3h,i). Thus, the DA release properties and the modulation of DA transmission by D2R autoreceptors are intact in this mouse model lacking D2Rs in striatal neurons.

Reduction of *in vivo* firing in the basal ganglia

Based on previous studies, we hypothesized that increased firing rate of iMSNs may account for the motor deficits of iMSN-Drd2KO mice (Hernandez-Lopez et al., 2000; Kravitz et al., 2010; Surmeier and Kitai, 1993). To test this hypothesis, we performed *in vivo* recordings in the dorsal striatum of freely moving control and iMSN-Drd2KO mice. Single unit recordings from MSNs and interneurons were sorted based on their waveform and firing rates (Figure S4). The same motor deficit was seen in iMSN-Drd2KO mice from whom we recorded single unit activity compared to control mice (Figure S4). The average firing rate per MSN was not significantly different between genotypes (Control: 0.86 ± 0.1 Hz; iMSN-Drd2KO: 0.76 ± 0.10 Hz, t-test, p = 0.42, n = 107–117 cells, Figure 4a,b). However, there was a significant variation in the number of cells recorded per animal, including a disproportionally large number of neurons recorded from one low firing control. We, therefore, assessed the average firing rate per animal, which was significantly lower in iMSN-Drd2KO mice relative to controls (Control: 0.91 ± 0.11 Hz; iMSN-Drd2KO: 0.46 ± 0.11 Hz, t-test, $p = 0.02$, n = 5–7 mice Figure 4c). Furthermore, there was no evidence of a bimodal distribution of firing rates in either genotype, indicating an overall decrease in firing rate across the two subpopulations of MSNs in iMSN-Drd2KO mice. To examine firing rates of iMSNs more specifically, we expressed channelrhodopsin (ChR2) in a cre-dependent manner and used optogenetic stimulation to identify single units arising specifically from iMSNs (optogenetic tagging). For these experiments, *Adora2A-Cre*$^{+/-}$ mice, which display similar locomotor activity as *Drd2*$^{loxP/loxP}$ littermates, were used as the control group (Figure S2). The firing rates of tagged iMSNs were also significantly lower in the iMSN-DrdKO mice (*Adora2A-Cre*$^{+/-}$: 0.91 ± 0.23 Hz vs. iMSN-DrdKO: 0.33 ± 0.11 Hz, one-tailed t-test, $p = 0.03$, n = 5–6 cells, Figure 4d–f), consistent with the results shown above. We were also able to record from a handful of putative GABAergic interneurons (based on fast waveform, Figure S4). There was also a significant decrease in firing in this putative interneuron population (Control: 16.1 ± 3.5 Hz; iMSN-Drd2KO: 4.6 ± 1.3 Hz, t-test, $p = 0.02$, n = 9–11 cells, Figure 4g). Taken together, we conclude that firing of both iMSNs and dMSNs are depressed in iMSN-Drd2KO mice in contrast to our prediction that firing of

iMSNs would be heightened following the loss of D2Rs. Furthermore, the reduction in putative interneuron firing indicates an overall depression in striatal network activity.

The *in vivo* firing of neurons in the globus pallidus external (GPe), the downstream target of iMSNs, was assessed next. There was a dramatic decrease in the firing rate of GPe neurons in iMSN-Drd2KO mice compared to controls (Control: 30.2 ± 5.1 Hz; iMSN-Drd2KO: 14.3 ± 2.4 Hz, $p = 0.002$, n = 35–49 cells, Figure 4h,i). This finding is consistent with the motor deficit of these mice but paradoxical when considering the decreased firing of iMSNs. To probe the cellular mechanism(s) underlying the changes in basal ganglia activity we turned to slice electrophysiology where we were able to isolate currents and selectively record from dMSNs and iMSNs.

Decreased excitability of iMSNs

Changes in intrinsic excitability of MSNs might contribute to the observed reduction of *in vivo* firing rate, particularly since it has been demonstrated that overexpression of D2Rs in the striatum enhances intrinsic excitability (Cazorla et al., 2012). *Drd2*$^{loxP/loxP}$ and iMSN-Drd2KO mice were crossed onto a *Drd1-tdTomato* background in order to identify D1R-positive MSNs (putative dMSNs) and D1R-negative MSNs (putative iMSNs) (Figure 5a,b). We confirmed that control *Drd1tdTmto;Drd2*$^{loxP/loxP}$ mice showed similar pattern of locomotor activity as *Drd2*$^{loxP/loxP}$ mice (Figure S2). The intrinsic excitability was measured using whole cell recordings from MSNs in brain slices in the presence of synaptic blockers. Consistent with previous studies (Chan et al., 2012; Kreitzer and Malenka, 2007), iMSNs showed higher intrinsic excitability than dMSNs in control *Drd1tdTmto;Drd2*$^{loxP/loxP}$ mice (current x cell type interaction, 2WRM ANOVA, $F_{12, 444} = 3.149$, $p = 0.0003$, n = 16–23). However, in iMSN-Drd2KO mice, there was a significant leftward shift in the current input-AP frequency relationship in iMSNs recorded from either the DS or the NAc demonstrating a reduction in excitability (DS: current x genotype interaction, 2WRM ANOVA, $F_{12,156} = 3.45$, $p < 0.0001$, n = 6–9, NAc: current x genotype interaction, 2WRM ANOVA, $F_{12,228} = 3.34$, $p = 0.0002$, n = 7–14, Figure 5c). The intrinsic excitability of dMSNs was similar between genotypes for both the DS and NAc (current x genotype interaction, 2WRM ANOVA, $ps > 0.05$, n = 5–9, Figure 6d). Thus, iMSNs were not more excitable than dMSNs in iMSN-Drd2KO mice.

These surprising findings prompted us to revisit the basic question of whether acute D2R activation can induce direct changes in membrane properties in the absence of synaptic inputs. We assessed the effect of acute application of the D2-like receptor agonist quinpirole (1 μM) on input-output curve of iMSNs in control mice in the presence of synaptic blockers. In cells recorded from either the DS or the NAc, acute quinpirole administration had no effect on the input-output curve of iMSNs (DS: current x drug interaction, 2WRM ANOVA, $F_{12,156} = 3.45$, $p = 0.84$, n = 6, NAc: current x drug interaction, 2WRM ANOVA, $F_{12,144} = 0.028$, $p = 1.0$, n = 7, Figure 5e). These findings indicate that acute D2R activation has no direct effect on the threshold to fire action potentials by iMSNs under these recording conditions.

The reduction of intrinsic excitability of iMSNs is consistent with reduced *in vivo* firing of these neurons and it could be the underlying mechanism. However, this result cannot

account for all the circuit perturbations observed in iMSN-Drd2KO mice such as the decrease in GPe firing and dMSN firing, two downstream targets of iMSNs. Recent studies have demonstrated an enhanced GABAergic tone within the basal ganglia following 6-OHDA lesion (Borgkvist et al., 2015; Fan et al., 2012). We therefore assessed the state of GABAergic transmission at the output of iMSNs.

Enhanced GABAergic transmission in the striatum and the GPe

We measured tonic and synaptic GABAergic transmission in putative dMSNs and iMSNs of *Drd2*$^{loxP/loxP}$ and iMSN-Drd2KO mice crossed with *Drd1-tdTomato* mice. For clarity, we combined data from the DS and NAc, when possible, and placed separated regional data in the supplement. GABA-A mediated tonic conductances have been studied across several brain regions and in the cerebellum and olfactory bulb have been found to be important regulators of neuronal excitability *in vivo*. High affinity GABA-A receptors, containing α5 or δ subunits underlie these tonic conductances, which are typically measured as a change in holding current of the cell as well as a change in current noise (Bright and Smart, 2013). The most consistent finding across striatal regions was the presence of a larger density of tonic inward current in dMSNs from iMSN-Drd2KO mice (0.6 ± 0.1 pA/pF for *Drd2*$^{loxP/loxP}$ vs. −1.0 ± 0.1 pA/pF for iMSN-Drd2KO; $p = 0.002$, n = 14–25; Figure 6a–c & S5,6). This increased tonic inward current is not due to changes in K^+ conductance since the recordings were performed using a Cs^+-based internal solution. The tonic inward current was inhibited by gabazine (10 μM) in both genotypes indicating that GABA-A receptor activation contributes to this current (one-sample t-tests vs. 100%, ps < 0.05). Importantly, the effect of gabazine on the tonic current was much more pronounced in iMSN-Drd2KO mice, effectively eliminating the difference in holding current density between controls and iMSN-Drd2KO mice (time x genotype interaction, 2WRM ANOVA, $F_{1,15} = 15.90$, $p = 0.0012$, n = 8–9, Figure 6d,e). Evaluating the data in another way, we found that gabazine blocked 25 ± 4% of the holding current recorded from dMSNs compared to only 11 ± 4% of the holding current recorded in dMSNs in control littermates *Drd2*$^{loxP/loxP}$ ($p < 0.011$, Figure 6f). There was no difference in tonic inward current between genotypes for either dMSNs or iMSNs in the presence of gabazine and when using 100% $CsMeSO_3$ based internal ($ps = 0.84, 0.86$ for dMSNs and iMSNs respectively, n = 12–16, Figure 6g). Thus, blocking GABA-A receptor mediated transmission revealed an enhanced tonic GABA-A mediated current in dMSNs from KO mice.

When examining fast synaptic GABA-A mediated transmission, we found that the frequency of miniature inhibitory postsynaptic currents (mIPSC) recorded from dMSNs was significantly increased in iMSN-Drd2KO mice (1.9 ± 0.2 Hz in *Drd2*$^{loxP/loxP}$ vs 2.4 ± 0.2 Hz in iMSN-Drd2KO: $p = 0.029$, n = 24–25). Similarly, mIPSC frequency was also increased in iMSNs (2.0± 0.2 Hz *for Drd2*$^{loxP/loxP}$ vs. 3.1 ± 0.3 Hz for iMSN-Drd2KO, $p = 0.0066$, n = 14–15; Figure 6h). The increased frequency was observed for small and large amplitude events, though it was most consistent for event amplitudes ranging from 10–30 pA (Figure 6i). The amplitude of mIPSCs was also increased in dMSNs (29 ± 2 pA for *Drd2*$^{loxP/loxP}$ vs 36 ± 3 pA for iMSN-Drd2KO, $p = 0.015$, n = 24–25, Figure 6h). Interestingly, there were cell-type specific regional differences throughout the striatum (Figure S5,6), which may be due to differences in the contribution of GABAergic inputs emanating from MSN axon

collaterals, interneurons and pallidal neurons onto MSNs to the overall mIPSC measurement. Yet this basic finding of enhanced fast synaptic GABAergic transmission was consistent between the DS and NAc. Taken together, these data demonstrate that deletion of D2Rs from iMSNs induces a robust enhancement of tonic and fast synaptic GABAergic transmission onto striatal neurons that may shunt excitation and contribute to decreased MSN firing *in vivo*.

We reasoned that if enhanced GABA release from iMSNs was contributing to the GABA tone in the striatum of IMSN-Drd2KO mice, a similar enhancement in GABAergic transmission should be observed in the GPe, the target of long-range projections from iMSNs. Under the exact same recording conditions as above, there was a robust increase in mIPSC frequency in GPe neurons recorded from iMSN-Drd2KO mice (6.6 ± 0.8 Hz in $Drd2^{loxP/loxP}$ vs 13.9 ± 2.4 Hz in iMSN-Drd2KO: $p = 0.005$, n = 17–19, Figure 6j–l). In contrast to the striatum, we did not find any change in amplitude (52.3 ± 3.0 pA in $Drd2^{loxP/loxP}$ vs 48.4 ± 3.0 Hz in iMSN-Drd2KO: $p = 0.37$, Figure 6l) or difference in holding current density (−1.1 ± 0.2 pA/pF in $Drd2^{loxP/loxP}$ vs −1.3 ± 0.3 pA/pF in iMSN-Drd2KO: $p = 0.69$, n = 17–19). This increase in mIPSC frequency, but not amplitude is consistent with an enhancement in probability of release at GABAergic terminals as a result of D2R deletion from iMSNs.

Miniature excitatory postsynaptic currents (mEPSC) were also recorded from iMSNs and dMSNs in the dorsal striatum. No change in mEPSC frequency (t-test, $p = 0.38$) nor amplitude ($p = 0.16$, n = 12–15, Figure S7) was found in iMSNs of iMSN-Drd2KO mice compared to littermate controls. Interestingly, we did observe a significant increase in mEPSC frequency in dMSNs ($p = 0.009$) and this was accompanied by a small, but significant change in mEPSC amplitude, ($p = 0.006$, n = 14–16, Figure S7). These data suggest a restructuring of glutamatergic connectivity following chronic D2R deletion from iMSNs. In general terms, these results are in agreement with results reported following dopamine depletion models but in those models the change was preferentially observed in iMSNs (Day et al., 2006; Kita and Kita, 2011).

Enhanced inhibition in the striatum drives the motor deficit

To test whether the enhanced intra-striatal GABAergic transmission was a key driver of the motor deficit observed in iMSN-Drd2KO mice, we conducted bilateral microinfusion experiments in which a small volume of a low dose of picrotoxin (125–150 nL, 100 μM) was infused into the striatum of $Drd2^{loxP/loxP}$ and iMSN-Drd2KO while locomotion was assessed. Mice were tethered to an infusion line and placed in an open field chamber (Figure 7a). Following a baseline period, mice were administered picrotoxin or vehicle (counterbalanced over two-days with a day off in between sessions) into the NAc or the DS (data is presented together because similar effects were found; Figure S5,6). Low dose picrotoxin administration had no significant effect on locomotion in control $Drd2^{loxP/loxP}$ mice compared to vehicle infusion (time x drug interaction, 2WRM ANOVA, $F_{10,140} = 1.023$, $p = 0.43$, n = 15, Figure 7a–c). In contrast, this same dose of picrotoxin was sufficient to enhance locomotion in iMSN-Drd2KO compared to vehicle infusion (time x drug interaction, 2WRM ANOVA, $F_{10,160} = 2.46$, $p = 0.009$, n = 16, Figure 7d). Indeed, after

small dose of picrotoxin iMSN-Drd2KO mice showed similar levels of locomotion compared to control animals (*Drd2*$^{loxP/loxP}$ – picrotoxin: 12.9 ± 2.0 m / 20 min vs. iMSN-Drd2KO – picrotoxin: 13.3 ± 2.2 m / 20 min, post-hoc test, $p = 0.98$, Figure 7e). Thus, these data provide strong evidence that the enhanced intra-striatal GABAergic transmission is a critical contributor to the motor deficit.

Activation of G_i-coupled DREADD in iMSNs reduced GABAergic transmission and restored motor output

D2Rs are G_i coupled receptors known to modulate neurotransmitter release at presynaptic terminals (Adrover et al., 2014; Dobbs, in press). We tested whether acute activation of G_i signaling in iMSNs could revert the enhanced GABAergic transmission observed in iMSN-Drd2KO mice back to control levels. The G_i-coupled DREADDs hM4Di were expressed in iMSNs of iMSN-Drd2KO mice (Figure 8a,c). The focus was in the NAc since this region showed increases in mIPSC frequency, amplitude and tonic current in dMSNs (Figure S6). First, the ability of hM4Di to inhibit iMSN output was confirmed by measuring isolated GABA transmission from iMSN collateral axons. In brain slices where iMSNs also co-expressed ChR2, recordings were made from neighboring putative dMSNs to measure optogenetically-evoked IPSCs (oIPSC). The synthetic hM4Di agonist CNO (1 μM) decreased oIPSCs by 85% (1W ANOVA, $F_{4,45} = 6.12$, $p = 0.0002$, n = 6, Figure 8a–b), demonstrating that G_i-DREADD activation can robustly inhibit isolated iMSN inputs onto dMSNs. In agreement with previous results, we found enhanced tonic inward currents and mIPSC frequency in dMSNs from these iMSN-Drd2KO mice. A short pre-incubation (10–15 min) with CNO resulted in an overall reduction in the holding current density in dMSNs from −1.2 ± 0.2 pA/pF to −0.7 ± 0.1 pA/pF in slices pre-incubated in ACSF alone and ACSF +CNO, respectively ($p = 0.045$, n = 23 per group; Figure 8c). Because reducing GABA transmission selectivity in iMSNs reduced the magnitude of tonic GABA-A mediated current, these results indicate that GABA release from iMSNs contributes to the enhanced inhibition observed in mice lacking D2Rs.

The same single acute administration of CNO had no effect on mIPSC amplitude nor frequency (amplitude: 33 ± 2.0 pA in ACSF alone vs. 30 ± 2.0 pA in ACSF+CNO, frequency: 2.0 ± 0.2 Hz in ACSF vs. 1.8 ± 0.2 Hz in ACSF+CNO; *ps* > 0.05; Figure 8c). This result suggests that other sources of GABAergic innervation are also strengthened and/or there is a requirement for chronic G_i signaling activation in order to achieve reversal of fast synaptic GABAergic transmission.

We also examined the effect of G_i-DREADD activation on GPe firing rate in iMSN-Drd2KO mice. In this experiment, iMSNs were transduced to express the Gi-DREADD based on modified kappa opioid receptor-DREADD called KORD (Vardy et al., 2015) and *in vivo* recordings of GPe neurons were performed before and after i.p. administration of vehicle or the KORD agonist SalvinorinB (SalB) (17 mg/kg i.p., dissolved in DMSO) (Figure 8d). There was a larger number of units that showed an increase in firing rate (>2 SD) after SalB administration (10/59 units) compared to vehicle (1/59 units); revealing a statistical trend for a drug increase in GPe firing (drug x time interaction, 2WRM ANOVA, $p = 0.12$, 59 units, 2

mice; Figure 8e–f). These data indicate that G_I signaling activation in iMSNs is sufficient to partially revert the decrease in GPe firing observed in iMSN-Drd2KO mice.

The next experiment tested whether Gi-DREADD activation in either the DS or NAc is sufficient to rescue the motor deficits of iMSN-Drd2KO mice. Before agonist administration, similar locomotion was seen in iMSN-Drd2KO mice expressing hM4Di or control mCherry in iMSNs in either the DS or NAc (Figures S8). Systemic administration of CNO (1 mg/kg, *i.p.*) 30 min prior to exposure to a novel open field caused a ~ 60% increase in total locomotor activity in iMSN-Drd2KO mice expressing hM4Di compared to those expressing mCherry in iMSNs ($ps < 0.05$, n = 8–11; Figure 9g–j). This was roughly the same locomotor activity observed in iMSN-Drd2HET mice. Similar increase in locomotion was observed whether the DS or NAc were targeted in iMSN-Drd2KO (Figure 8g–j). CNO mainly increased the sustained locomotion by ~70% ($ps < 0.05$, Figure 8g–j, S8). Interestingly, this manipulation had no significant effect on the novel exploration phase of locomotor response ($ps > 0.05$; Figure 8g–j, S8). It should be noted that activation of KORD by SalB during the GPe firing experiment also increased locomotion in iMSN-Drd2KO mice (Figure S8). Thus, altogether the activation of Gi-DREADD receptors only in iMSNs suppressed the enhanced tonic GABAergic transmission in the striatum and rescued the locomotor deficit observed in iMSN-Drd2KO mice.

Finally, we tested whether intra-striatal activation of G_i-DREADD in iMSNs could rescue the motor deficit. Bilateral cannulas were implanted in DS of iMSN-Drd2KO mice expressing hM4Di or control mCherry in iMSNs (Figure 8k,l). Mice were habituated to being tethered and the open field chamber for several sessions before the testing began. iMSN-Drd2KO mice expressing mCherry in the DS served as control and showed a typical time-dependent reduction in locomotion that is referred to as habituation following CNO microinfusion of (10 μM, 300 nL/side). In contrast, iMSN-Drd2KO mice expressing hM4Di showed a sustain increase in locomotion across time after CNO microinfusion, which prevented habituation (Figure 9m). The average speed (m/5 min) was significantly higher in iMSN-Drd2KO mice expressing hM4Di than mCherry during the last 20 min post CNO microinfusion (2.37 ± 0.53 vs 1.3 ± 0.26 m/5 min for hM4Di and mCherry, respectively; one-tailed t-test, $p = 0.044$, n = 9–10).

Discussion

Selective deletion of D2Rs from iMSNs resulted in hypokenisa and bradykinesia, two characteristic motor deficits observed in Parkinson's disease patients and DA depletion models of Parkinson's disease (Smith et al., 2013). These locomotor deficits are ameliorated in the presence of salient stimuli, resembling the paradoxical kinesia observed in Parkinson's patients (Bienkiewicz et al., 2013) and also in agreement with observations made in DA depletion models of Parkinson's disease (Keefe et al., 1989; Rodriguez Diaz et al., 2001). However, in contrast to Parkinson's patients and DA depletion models, mice lacking D2Rs in iMSNs show normal DA levels and release properties. Thus, this targeted deletion approach has allowed us to dissect the selective contribution of this particular subpopulation of D2Rs within the basal ganglia to the regulation of motor output. The results show that activation of D2Rs in iMSNs are required for sustained locomotion.

D2Rs in iMSNs were shown to suppress lateral inhibition between MSNs (Dobbs, in press; Tecuapetla et al., 2009). These receptors are exquisitely positioned to exert potent control over MSN excitability and striatal output via regulation of GABA release. Indeed, we show that excision of D2Rs from iMSNs enhances inhibitory transmission in the striatum and the GPe and decreases *in vivo* MSN and GPe firing in awake behaving animal. Interestingly, we showed that the D2-like agonist quinpirole does not alter the intrinsic excitability of iMSNs recorded from control animals in the presence of synaptic blockers suggesting that regulation of somatodendritic ion channel conductances may not be the primary action of D2Rs in the striatum. Several studies using 6-OHDA lesions have reported an increase in MSN firing rate following DA depletion (Chen et al., 2001; Hull et al., 1974; Kish et al., 1999; Tseng et al., 2001), in contrast to our observations. However, in agreement with our findings, other studies have observed decreased firing (Chan et al., 2012; Chang et al., 2006). Also in support of our results, treatment with a D2 antagonist reproduced the reduction in MSN firing *in vitro* (Chan et al., 2012) and in freely moving rats (Yael et al., 2013). The diverse results in the MSN firing data may be due to variations in the extent and duration of the DA depletion, which in turn could affect the degree of compensation such as upregulation of D2Rs in MSNs (Brene et al., 1994; Cadet et al., 1992; Narang and Wamsley, 1995; Schultz and Ungerstedt, 1978), a compensatory mechanism that cannot occur in our mouse model.

The prediction from the classic “go-no go” model is that increased output of the indirect pathway with concurrent decreased output of the direct pathway underlies the motor impairments of DA depletion and found in Parkinson’s disease patients. Although our observations appear to contradict this model at first glance, enhanced *firing* of iMSNs is only one possible mechanism for increasing indirect pathway output. Our data points to a dissociation between excitability/firing measured at the soma and GABA release measured from synaptic terminals. It suggests that GABA transmission from iMSNs is enhanced in iMSN-Drd2KO mice, despite decreased iMSN intrinsic excitability and baseline *in vivo* firing.

Our results are also consistent with the “go-no go” model in that they indicate a decrease in direct pathway output. However, in this case the reduction in dMSN output is largely due to hyper-GABAergic tone generated by a loss of D2R regulation. This hypothesis is supported by the results of the G_i-DREADD rescue experiment (Figure 8) in which acute activation of Gi-DREADDs in iMSNs reduced the size of the GABA-A mediated tonic current measured in dMSNs and enhanced locomotion in iMSN-Drd2KO mice. It is also important to note that other sources of GABA release in the striatum are likely to be potentiated and contribute to the phenotype, such as stronger FSI ➔MSN and GPe feed forward connectivity, as reported following 6-OHDA lesions (Fan et al., 2012; Gittis et al., 2011). Independently of the source of GABA, our data favors the idea of a causal relationship between the enhanced GABA transmission and the decreased firing of both dMSNs and iMSNs leading to motor output deficits.

In summary, this study highlights the importance of DA regulation of intra-striatal inhibitory connectivity by D2Rs often referred as “postsynaptic” DA receptors. Here the results highlight its role at the level of presynaptic GABAergic terminals, as opposed to in the

somata and dendrites, where these striatal D2Rs can potently suppress lateral inhibition and facilitate locomotion. This mechanism is rarely considered in the current models of basal ganglia function yet should be integrated in order to improve our understanding of this complex circuitry and the development of therapeutics for DA-related disease states.

Experimental Procedures

All procedures were performed in accordance with guidelines from the Animal Care and Use Committee of the National Institute on Alcohol Abuse and Alcoholism or the National Institute for Diabetes and Digestive and Kidney Diseases.

Animals

Mice (p60–180) were group housed unless otherwise specified and kept under a 12h-light cycle (6:30 ON/18:30 OFF) with food and water available *ad libitum*. For list of mouse lines, sources and citations see Supplementary Experimental Procedures.

Behavior

For all procedures required, mice were moved to behavioral suite and allowed to acclimate for at least 30 min and, if handling was required, mice were handled 3–5 days prior to testing for habituation. ***Locomotion and exploration***: Homecage locomotion was measured in mice that were individually housed several weeks prior to measurements. Mice were acclimated to the behavioral suite for 48 hs and then locomotion was measured using beam break detectors (Opto-M4, Columbus Instruments) for 2 consecutive days and averaged for 24 hs. Open-field locomotion was measured in small (20 h × 17 w × 28 l cm) polycarbonate chambers for 1hr using beak break detectors or in a large (40 × 40 × 40 cm) acrylic/PVC chambers for 30 min using video monitoring.. ***Locomotion in air- and water-filled chambers***: Opaque plastic circular chambers (20 cm diameter) were filled with warm water (30°C) or air. Each mouse was tested in two sessions (water and air counterbalanced across a two-day period) and video monitored for 15 min. Videos were analyzed using Noldus Ethovision and mobility was defined as speed > 2 cm/s over 15 sample frames while immobility defined by speed < 0.75cm/s. ***Intra-striatal microinfusion of picrotoxin***: Mice were tethered to an infusion line and placed in large open-field chamber for 45-min baseline period. ACSF (vehicle) or picrotoxin (100 μM; counterbalanced across two days) was infused bilaterally via the cannula into the striatum (125–150 nL/side at 100 nL/min) and locomotion was assessed during 25 min post-infusion. ***Novel object Exploration***: Mice were habituated to large open-field chamber for 30 min and returned to homecage for 5 min, during which time a novel object was placed in the center of the open field. Animals were placed back into chamber and allowed to explore for 15 min while video recording. ***Gi-DREADD locomotion rescue***: For systemic administration, mice received of CNO (1 mg/kg, *i.p.*, in saline) in their homecage 30 min prior to being placed in large open-field chamber for 30 min. For intracranial administration, CNO (10 μM in ACSF) was infused via the cannula bilaterally (300 nL at 100 nL/min) while the animal was in the homecage and the drug was allowed to diffuse for an additional 3 min after infusion was completed. Animals were then placed (untethered) in the large open-field chamber for 70 min. Videos were analyzed using Noldus Ethovision software and total distance travel and speed

calculated. ***Accelerating Rotarod***: Mice were habituated to the rotarod (MedAssociates) for 1 min at 4 rpm. Following habituation, the rotarod accelerated from 4 to 40 rpm over 300 seconds. The trial was terminated at 300 sec. Each trial was separated by ~20 min and there were six trials on day 1, followed by 4 trials on day 2–6. Additional details at Supplemental Procedures.

In vitro electrophysiology

Sagittal slices (240 μm) containing the dorsomedial striatum and NAc core were prepared from 8–16 week-old mice from the *Drd2*$^{loxP/loxP}$ and iMSN-Drd2KO line that were crossed into a *Drd1-tdTomato* line. Slices were cut in ice-cold cutting solution (in mM): 225 sucrose, 13.9 NaCl, 26.2 $NaHCO_3$, 1 NaH_2PO_4, 1.25 glucose, 2.5 KCl, 0.1 $CaCl_2$, 4.9 $MgCl_2$, and 3 kynurenic acid. Slices were maintained in oxygenated ACSF containing (in mM): 124 NaCl, 2.5 KCl, 2.5 $CaCl_2$, 1.3 $MgCl_2$, 26.2 $NaHCO_3$, 1 NaH_2PO_4, and 20 glucose (~310–315 mOsm) at RT following a 1hr recovery period at 33°C. Whole-cell voltage clamp experiments were performed to measure electrically evoked IPSCs, mIPSCs and mEPSCs and current clamp experiments for intrinsic excitability. See Supplementary Experimental Procedures for list of internal solutions and drugs used for each experiment. Data were acquired at 5 kHz and filtered at 1 kHz using Multiclamp 700B (Molecular Devices). Data was analyzed using pClamp (Clampfit, v. 10.3) and MiniAnalysis (Synaptosoft, Inc.).

Fast scanning cyclic voltammetry

Brain slices and solutions were prepared as described in the electrophysiology section and recordings performed as previously described (Adrover et al., 2014). The carbon-fiber electrode was held at −0.4 V and a voltage ramp to and from 1.2 V (400V/s) was delivered every 100 ms (10 Hz). Before recording, electrodes were conditioned by running the ramp at 60 Hz for 15 min and at 10 Hz for another 15 min and calibrated. Electrodes were calibrated using 1 μM DA. DA transients were evoked by electrical stimulation delivered through a glass microelectrode filled with ACSF. Either a single monophasic pulse (0.2 msec, 300 μA) or train of pulses (20 pulses, 20Hz) was delivered to the slice in the absence or presence of the D2R antagonist sulpiride (1 μM). Data was acquired with a retrofitted headstage and Axon Amplifier using Multiclamp. Voltammetric analysis was done using custom written procedures in Igor Pro software.

In vivo Electrophysiology

iMSN-Drd2KO and control (*Adora2A-Cre*$^{+/-}$ or *Drd2*$^{loxP/loxP}$) mice were anesthetized with chloral hydrate (380 mg/kg) during surgery. One array of 32 Teflon-coated tungsten microwires (35 μm diameter) was implanted unilaterally in striatum (A/P: +0.8, Lat: +1.5, D/V: −2.6 mm from top of skull) or the globus pallidus (A/P: −0.5, Lat: +2.0, D/V: −3.5 from top of skull) and a stainless steel ground wire was implanted under the skull. For recordings, animals were placed in plastic chamber (25 cm diameter) or a novel mouse cage, and allowed to move freely. In a subset of animals, ChR2 or KORD was also infused into the striatum (0.1mm deeper than array) during surgery. Single units were discriminated using principal component analysis (Offline Sorter; Plexon). Spike channels were acquired at 40kHz with 16 bit resolution, and the signal was band pass filtered at 150 Hz-8 kHz before

spike sorting. Medium spiny neurons and interneurons were identified based on waveform shape and average firing rate, similar to what has previously been described (Berke et al., 2004). High-quality single unit isolation was achieved, as assessed by measures of spike-sorting quality (Wheeler 1998) Davies–Bouldin index, J3 statistic.

Immunohistochemistry

Mice were intracardially perfused with PBS containing 10U/mL Heparin until the liver cleared (~ 5 min) followed by 40 ml fixative solution (4% paraformaldehyde; 4% sucrose in 0.1M PB) at 3 ml/min. Brain was removed, post-fixed overnight and then kept in 30% sucrose in 0.1M PB. Coronal or sagittal floating sections (40 μm) were prepared using cryostat (Leica CM3050). Floating sections were washed in PBS and then blocked for 1h in 5% normal goat or donkey serum, 0.3% Triton-X in PBS at RT. Sections were then incubated in primary antibody for 12–18hrs at RT. Following 3 × 10 min washes in PBS, sections were incubated in goat or donkey secondary antibodies conjugated with AlexaFluor (1:500, Invitrogen) for 2 hr at RT. For a full list of antibodies, concentrations, and sources see Supplemental Procedures. Slices were washed 3 × 10 min in PBS, then 2 × 10 min in 0.1M PB. Images (512×512 or 1024×1024) were acquired using a confocal microscope (Zeiss LSM 510 META, Thornwood, NY) and analyzed using ImageJ (NIH).

Statistics

Statistical analysis was performed in Prism (GraphPad) and Excel. Unless stated, two-tailed unpaired t-test was used. Otherwise, two-tailed paired t-test, 1W ANOVAs or 2W Repeated Measures (2WRM) ANOVAs or one-tailed t-tests were used when appropriate and stated. 2W ANOVAs were followed up with Sidak-corrected t-test comparisons. All data are presented as mean ± SEM. Results were considered significant at an alpha of 0.05.

Supplementary Material

Refer to Web version on PubMed Central for supplementary material.

Acknowledgments

Funded by Intramural Research Programs of NIAAA, NINDS (ZIA-AA000421) to VAA; NIDDK (ZIA-DK075096) to AVK; NIGMS and PRAT fellowship to JCL; ANPCYT-Mincyt, Universidad de Buenos Aires and Tourette Syndrome Association to MR. We are grateful to Roland Bock who wrote the Igor procedures used for voltammetry and to Dr. Ono for sharing confocal microscope. We thank Dr. Lovinger and members of the Alvarez lab for helpful comments and Drs. Roth (UNC) and Deisseroth (Stanford) for generously provided hM4Di and ChR2 constructs.

References

Adrover MF, Shin JH, Alvarez VA. Glutamate and dopamine transmission from midbrain dopamine neurons share similar release properties but are differentially affected by cocaine. The Journal of neuroscience : the official journal of the Society for Neuroscience. 2014; 34:3183–3192. [PubMed: 24573277]

Albin RL, Young AB, Penney JB. The functional anatomy of basal ganglia disorders. Trends Neurosci. 1989; 12:366–375. [PubMed: 2479133]

Anzalone A, Lizardi-Ortiz JE, Ramos M, De Mei C, Hopf FW, Iaccarino C, Halbout B, Jacobsen J, Kinoshita C, Welter M, et al. Dual control of dopamine synthesis and release by presynaptic and

postsynaptic dopamine D2 receptors. The Journal of neuroscience : the official journal of the Society for Neuroscience. 2012; 32:9023–9034. [PubMed: 22745501]

Baik JH, Picetti R, Saiardi A, Thiriet G, Dierich A, Depaulis A, Le Meur M, Borrelli E. Parkinsonian-like locomotor impairment in mice lacking dopamine D2 receptors. Nature. 1995; 377:424–428. [PubMed: 7566118]

Bamford NS, Zhang H, Schmitz Y, Wu NP, Cepeda C, Levine MS, Schmauss C, Zakharenko SS, Zablow L, Sulzer D. Heterosynaptic dopamine neurotransmission selects sets of corticostriatal terminals. Neuron. 2004; 42:653–663. [PubMed: 15157425]

Bateup HS, Santini E, Shen W, Birnbaum S, Valjent E, Surmeier DJ, Fisone G, Nestler EJ, Greengard P. Distinct subclasses of medium spiny neurons differentially regulate striatal motor behaviors. Proceedings of the National Academy of Sciences of the United States of America. 2010; 107:14845–14850. [PubMed: 20682746]

Bello EP, Mateo Y, Gelman DM, Noain D, Shin JH, Low MJ, Alvarez VA, Lovinger DM, Rubinstein M. Cocaine supersensitivity and enhanced motivation for reward in mice lacking dopamine D2 autoreceptors. Nature neuroscience. 2011; 14:1033–1038. [PubMed: 21743470]

Bergman H, Deuschl G. Pathophysiology of Parkinson's disease: from clinical neurology to basic neuroscience and back. Movement disorders : official journal of the Movement Disorder Society. 2002; 17(Suppl 3):S28–40. [PubMed: 11948753]

Berke JD, Okatan M, Skurski J, Eichenbaum HB. Oscillatory entrainment of striatal neurons in freely moving rats. Neuron. 2004; 43:883–896. [PubMed: 15363398]

Bienkiewicz MM, Rodger MW, Young WR, Craig CM. Time to get a move on: overcoming bradykinetic movement in Parkinson's disease with artificial sensory guidance generated from biological motion. Behav Brain Res. 2013; 253:113–120. [PubMed: 23838076]

Borgkvist A, Avegno EM, Wong MY, Kheirbek MA, Sonders MS, Hen R, Sulzer D. Loss of Striatonigral GABAergic Presynaptic Inhibition Enables Motor Sensitization in Parkinsonian Mice. Neuron. 2015; 87:976–988. [PubMed: 26335644]

Brene S, Herrera-Marschitz M, Persson H, Lindefors N. Expression of mRNAs encoding dopamine receptors in striatal regions is differentially regulated by midbrain and hippocampal neurons. Brain research. Molecular brain research. 1994; 21:274–282. [PubMed: 8170351]

Bright DP, Smart TG. Methods for recording and measuring tonic GABAA receptor-mediated inhibition. Front Neural Circuits. 2013; 7:193. [PubMed: 24367296]

Cadet JL, Zhu SM, Angulo JA. Quantitative in situ hybridization evidence for differential regulation of proenkephalin and dopamine D2 receptor mRNA levels in the rat striatum: effects of unilateral intrastriatal injections of 6-hydroxydopamine. Brain research Molecular brain research. 1992; 12:59–67. [PubMed: 1312206]

Cazorla M, Shegda M, Ramesh B, Harrison NL, Kellendonk C. Striatal D2 receptors regulate dendritic morphology of medium spiny neurons via Kir2 channels. The Journal of neuroscience : the official journal of the Society for Neuroscience. 2012; 32:2398–2409. [PubMed: 22396414]

Centonze D, Grande C, Usiello A, Gubellini P, Erbs E, Martin AB, Pisani A, Tognazzi N, Bernardi G, Moratalla R, et al. Receptor subtypes involved in the presynaptic and postsynaptic actions of dopamine on striatal interneurons. The Journal of neuroscience : the official journal of the Society for Neuroscience. 2003; 23:6245–6254. [PubMed: 12867509]

Chan CS, Peterson JD, Gertler TS, Glajch KE, Quintana RE, Cui Q, Sebel LE, Plotkin JL, Shen W, Heiman M, et al. Strain-specific regulation of striatal phenotype in Drd2-eGFP BAC transgenic mice. The Journal of neuroscience : the official journal of the Society for Neuroscience. 2012; 32:9124–9132. [PubMed: 22764222]

Chang JY, Shi LH, Luo F, Woodward DJ. Neural responses in multiple basal ganglia regions following unilateral dopamine depletion in behaving rats performing a treadmill locomotion task. Exp Brain Res. 2006; 172:193–207. [PubMed: 16369786]

Chen MT, Morales M, Woodward DJ, Hoffer BJ, Janak PH. In vivo extracellular recording of striatal neurons in the awake rat following unilateral 6-hydroxydopamine lesions. Exp Neurol. 2001; 171:72–83. [PubMed: 11520122]

Cho J, Duke D, Manzino L, Sonsalla PK, West MO. Dopamine depletion causes fragmented clustering of neurons in the sensorimotor striatum: evidence of lasting reorganization of corticostriatal input. J Comp Neurol. 2002; 452:24–37. [PubMed: 12205707]

Costa RM, Lin SC, Sotnikova TD, Cyr M, Gainetdinov RR, Caron MG, Nicolelis MA. Rapid alterations in corticostriatal ensemble coordination during acute dopamine-dependent motor dysfunction. Neuron. 2006; 52:359–369. [PubMed: 17046697]

Day M, Wang Z, Ding J, An X, Ingham CA, Shering AF, Wokosin D, Ilijic E, Sun Z, Sampson AR, et al. Selective elimination of glutamatergic synapses on striatopallidal neurons in Parkinson disease models. Nat Neurosci. 2006; 9:251–259. [PubMed: 16415865]

DeLong MR. Activity of basal ganglia neurons during movement. Brain Res. 1972; 40:127–135. [PubMed: 4624486]

Delong MR, Georgopoulos AP, Crutcher MD, Mitchell SJ, Richardson RT, Alexander GE. Functional organization of the basal ganglia: contributions of single-cell recording studies. Ciba Foundation symposium. 1984; 107:64–82. [PubMed: 6389041]

Deumens R, Blokland A, Prickaerts J. Modeling Parkinson's disease in rats: an evaluation of 6-OHDA lesions of the nigrostriatal pathway. Experimental neurology. 2002; 175:303–317. [PubMed: 12061862]

Dobbs L, Kaplan AR, Lemos JC, Matsui A, Rubinstein M, Alvarez VA. Dopamine regulation of lateral inhibition between striatal neurons gates the stimulant actions of cocaine. in press.

Durieux PF, Bearzatto B, Guiducci S, Buch T, Waisman A, Zoli M, Schiffmann SN, de Kerchove d'Exaerde A. D2R striatopallidal neurons inhibit both locomotor and drug reward processes. Nature neuroscience. 2009; 12:393–395. [PubMed: 19270687]

Durieux PF, Schiffmann SN, de Kerchove d'Exaerde A. Differential regulation of motor control and response to dopaminergic drugs by D1R and D2R neurons in distinct dorsal striatum subregions. The EMBO journal. 2012; 31:640–653. [PubMed: 22068054]

Fan KY, Baufreton J, Surmeier DJ, Chan CS, Bevan MD. Proliferation of external globus pallidus-subthalamic nucleus synapses following degeneration of midbrain dopamine neurons. The Journal of neuroscience : the official journal of the Society for Neuroscience. 2012; 32:13718–13728. [PubMed: 23035084]

Fink JS, Smith GP. Mesolimbicocortical dopamine terminal fields are necessary for normal locomotor and investigatory exploration in rats. Brain Res. 1980; 199:359–384. [PubMed: 7417789]

Gallo EF, Salling MC, Feng B, Moron JA, Harrison NL, Javitch JA, Kellendonk C. Upregulation of Dopamine D2 Receptors in the Nucleus Accumbens Indirect Pathway Increases Locomotion but does not Reduce Alcohol Consumption. Neuropsychopharmacology. 2015

Gerfen CR, Surmeier DJ. Modulation of striatal projection systems by dopamine. Annu Rev Neurosci. 2011; 34:441–466. [PubMed: 21469956]

Gittis AH, Hang GB, LaDow ES, Shoenfeld LR, Atallah BV, Finkbeiner S, Kreitzer AC. Rapid target-specific remodeling of fast-spiking inhibitory circuits after loss of dopamine. Neuron. 2011; 71:858–868. [PubMed: 21903079]

Hernandez-Lopez S, Tkatch T, Perez-Garci E, Galarraga E, Bargas J, Hamm H, Surmeier DJ. D2 dopamine receptors in striatal medium spiny neurons reduce L-type Ca2+ currents and excitability via a novel PLC[beta]1-IP3-calcineurin-signaling cascade. The Journal of neuroscience : the official journal of the Society for Neuroscience. 2000; 20:8987–8995. [PubMed: 11124974]

Hull CD, Levine MS, Buchwald NA, Heller A, Browning RA. The spontaneous firing pattern of forebrain neurons. I. The effects of dopamine and non-dopamine depleting lesions on caudate unit firing patterns. Brain Res. 1974; 73:241–262. [PubMed: 4151549]

Keefe KA, Salamone JD, Zigmond MJ, Stricker EM. Paradoxical kinesia in parkinsonism is not caused by dopamine release. Studies in an animal model. Archives of neurology. 1989; 46:1070–1075. [PubMed: 2508609]

Kelly MA, Rubinstein M, Phillips TJ, Lessov CN, Burkhart-Kasch S, Zhang G, Bunzow JR, Fang Y, Gerhardt GA, Grandy DK, Low MJ. Locomotor activity in D2 dopamine receptor-deficient mice is determined by gene dosage, genetic background, and developmental adaptations. The Journal of neuroscience : the official journal of the Society for Neuroscience. 1998; 18:3470–3479. [PubMed: 9547254]

Kish LJ, Palmer MR, Gerhardt GA. Multiple single-unit recordings in the striatum of freely moving animals: effects of apomorphine and D-amphetamine in normal and unilateral 6-hydroxydopamine-lesioned rats. Brain Res. 1999; 833:58–70. [PubMed: 10375677]

Kita H, Kita T. Cortical stimulation evokes abnormal responses in the dopamine-depleted rat basal ganglia. The Journal of neuroscience : the official journal of the Society for Neuroscience. 2011; 31:10311–10322. [PubMed: 21753008]

Kravitz AV, Freeze BS, Parker PR, Kay K, Thwin MT, Deisseroth K, Kreitzer AC. Regulation of parkinsonian motor behaviours by optogenetic control of basal ganglia circuitry. Nature. 2010; 466:622–626. [PubMed: 20613723]

Kreitzer AC, Malenka RC. Endocannabinoid-mediated rescue of striatal LTD and motor deficits in Parkinson's disease models. Nature. 2007; 445:643–647. [PubMed: 17287809]

Legault M, Wise RA. Novelty-evoked elevations of nucleus accumbens dopamine: dependence on impulse flow from the ventral subiculum and glutamatergic neurotransmission in the ventral tegmental area. Eur J Neurosci. 2001; 13:819–828. [PubMed: 11207817]

Lovinger DM. Neurotransmitter roles in synaptic modulation, plasticity and learning in the dorsal striatum. Neuropharmacology. 2010; 58:951–961. [PubMed: 20096294]

Maurice N, Mercer J, Chan CS, Hernandez-Lopez S, Held J, Tkatch T, Surmeier DJ. D2 dopamine receptor-mediated modulation of voltage-dependent Na+ channels reduces autonomous activity in striatal cholinergic interneurons. The Journal of neuroscience : the official journal of the Society for Neuroscience. 2004; 24:10289–10301. [PubMed: 15548642]

Narang N, Wamsley JK. Time dependent changes in DA uptake sites, D1 and D2 receptor binding and mRNA after 6-OHDA lesions of the medial forebrain bundle in the rat brain. Journal of chemical neuroanatomy. 1995; 9:41–53. [PubMed: 8527037]

Palmiter RD. Dopamine signaling in the dorsal striatum is essential for motivated behaviors: lessons from dopamine-deficient mice. Annals of the New York Academy of Sciences. 2008; 1129:35–46. [PubMed: 18591467]

Rodriguez Diaz M, Abdala P, Barroso-Chinea P, Obeso J, Gonzalez-Hernandez T. Motor behavioural changes after intracerebroventricular injection of 6-hydroxydopamine in the rat: an animal model of Parkinson's disease. Behav Brain Res. 2001; 122:79–92. [PubMed: 11287079]

Rubinstein M, Muschietti JP, Gershanik O, Flawia MM, Stefano FJ. Adaptive mechanisms of striatal D1 and D2 dopamine receptors in response to a prolonged reserpine treatment in mice. The Journal of pharmacology and experimental therapeutics. 1990; 252:810–816. [PubMed: 2138223]

Schultz W. Depletion of dopamine in the striatum as an experimental model of Parkinsonism: direct effects and adaptive mechanisms. Progress in neurobiology. 1982; 18:121–166. [PubMed: 6813911]

Schultz W, Ungerstedt U. Short-term increase and long-term reversion of striatal cell activity after degeneration of the nigrostriatal dopamine system. Exp Brain Res. 1978; 33:159–171. [PubMed: 700003]

Smith RJ, Lobo MK, Spencer S, Kalivas PW. Cocaine-induced adaptations in D1 and D2 accumbens projection neurons (a dichotomy not necessarily synonymous with direct and indirect pathways). Curr Opin Neurobiol. 2013; 23:546–552. [PubMed: 23428656]

Surmeier DJ, Carrillo-Reid L, Bargas J. Dopaminergic modulation of striatal neurons, circuits, and assemblies. Neuroscience. 2011; 198:3–18. [PubMed: 21906660]

Surmeier DJ, Graves SM, Shen W. Dopaminergic modulation of striatal networks in health and Parkinson's disease. Curr Opin Neurobiol. 2014; 29C:109–117. [PubMed: 25058111]

Surmeier DJ, Kitai ST. D1 and D2 dopamine receptor modulation of sodium and potassium currents in rat neostriatal neurons. Prog Brain Res. 1993; 99:309–324. [PubMed: 7906427]

Tecuapetla F, Koos T, Tepper JM, Kabbani N, Yeckel MF. Differential dopaminergic modulation of neostriatal synaptic connections of striatopallidal axon collaterals. The Journal of neuroscience : the official journal of the Society for Neuroscience. 2009; 29:8977–8990. [PubMed: 19605635]

Tseng KY, Kasanetz F, Kargieman L, Riquelme LA, Murer MG. Cortical slow oscillatory activity is reflected in the membrane potential and spike trains of striatal neurons in rats with chronic nigrostriatal lesions. The Journal of neuroscience : the official journal of the Society for Neuroscience. 2001; 21:6430–6439. [PubMed: 11487667]

Vandeputte C, Taymans JM, Casteels C, Coun F, Ni Y, Van Laere K, Baekelandt V. Automated quantitative gait analysis in animal models of movement disorders. BMC neuroscience. 2010; 11:92. [PubMed: 20691122]

Vardy E, Robinson JE, Li C, Olsen RH, DiBerto JF, Giguere PM, Sassano FM, Huang XP, Zhu H, Urban DJ, et al. A New DREADD Facilitates the Multiplexed Chemogenetic Interrogation of Behavior. Neuron. 2015; 86:936–946. [PubMed: 25937170]

Yael D, Zeef DH, Sand D, Moran A, Katz DB, Cohen D, Temel Y, Bar-Gad I. Haloperidol-induced changes in neuronal activity in the striatum of the freely moving rat. Front Syst Neurosci. 2013; 7:110. [PubMed: 24379762]

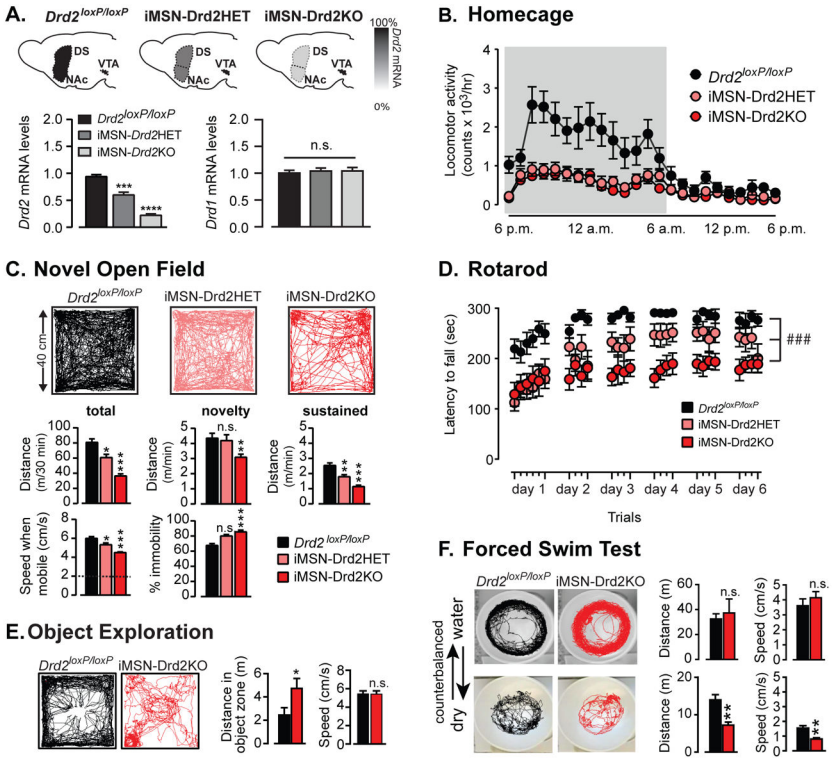

Figure 1. Targeted deletion of D2Rs to iMSNs produces deficit in spontaneous movement and motor skill performance

a) *Top,* Schematic of transgenic mouse lines generated: control *Drd2*$^{loxP/loxP}$ mice and mice with a single-allele deletion of *Drd2* gene (iMSN-Drd2Het) and both allele-deletion (iMSN-Drd2KO) in striatal iMSNs. *Bottom*, Striatal levels of *Drd2* and *Drd1* mRNA measured with qPCR in iMSN-Drd2HET and iMSN-Drd2KO mice relative to *Drd2*$^{loxP/loxP}$ mice, *** $p <$ 0.001 and **** $p < 0.0001$; n = 3–3–5. **b**) Locomotion measured in homecage for *Drd2*$^{loxP/loxP}$ (black), iMSN-Drd2HET (pink) and iMSN-Drd2KO (red) mice, n = 9–14. **c**) *Top*, Representative track traces for the three genotypes. *Middle*, Total distance traveled over 30 min, during first minute ("novelty phase"), and average speed during last 20 min ("sustained phase") for the three genotypes. *Bottom*, Speed when mobile (dashed line at 2cm/s threshold) and percent time immobile for the three genotypes*; n* = 9–28, *,**,*** *ps* < 0.05, 0.01 and 0.001 respectively in post-hoc t-tests. **d**) Latency to fall in the rotarod assay for the three genotypes; n = 8–10, ### genotype x latency interaction $p < 0.001$. **e**) Representative traces, average speed and total distance of exploratory behavior around novel object for *Drd2*$^{loxP/loxP}$ and iMSN-Drd2KO, n = 20–21, * t-test, $p < 0.05$. **f**) Representative traces, total distance traveled and average speed for *Drd2*$^{loxP/loxP}$ and iMSN-Drd2KO animals in the forced swim test, n = 9–11. ** t-test, $p < 0.01$.

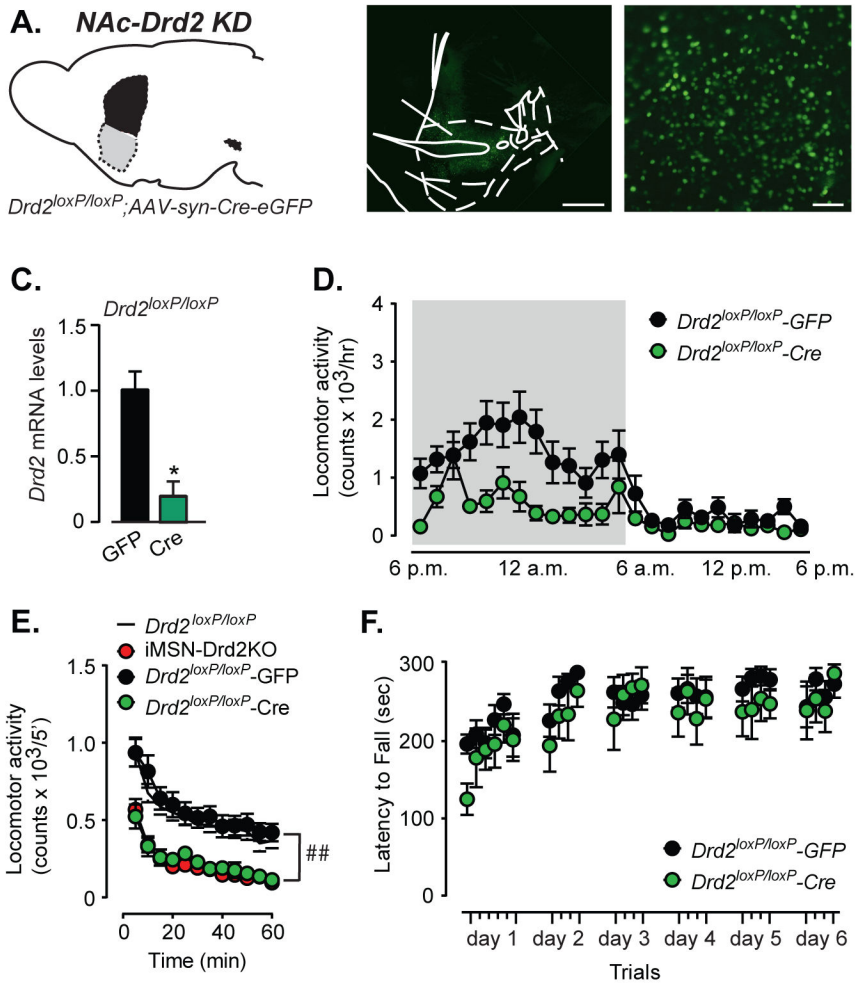

Figure 2. Knock-down of D2Rs in NAc core impairs horizontal locomotion but not rotarod performance

a) Schematic of NAc-specific knock-down of *Drd2* gene. **b**) Low and high power magnification images of brain sections from *Drd2*$^{loxP/loxP}$mice showing Cre-GFP expression in NAc. **c**) Striatal *Drd2* mRNA levels in *Drd2*$^{loxP/loxP}$ mice expressing Cre relative to control GFP mice, n = 2–2, * t-test, $p < 0.05$. **d**) Locomotion in homecage over a 24 h light-dark cycle for *Drd2*$^{loxP/loxP}$–Cre and *Drd2*$^{loxP/loxP}$–GFP mice, n = 5–9. **e**) Locomotion in small novel chamber for naive *Drd2*$^{loxP/loxP}$ (white), *Drd2*$^{loxP/loxP}$ – Cre (green), *Drd2*$^{loxP/loxP}$ – GFP (black) and iMSN-Drd2KO (red) mice over a 1 h period, n = 12–18, ## time x genotype interaction, $p < 0.01$. **f**) Latency to fall during rotarod test for *Drd2*$^{loxP/loxP}$ -Cre and *Drd2*$^{loxP/loxP}$-GFP mice, n = 6–9.

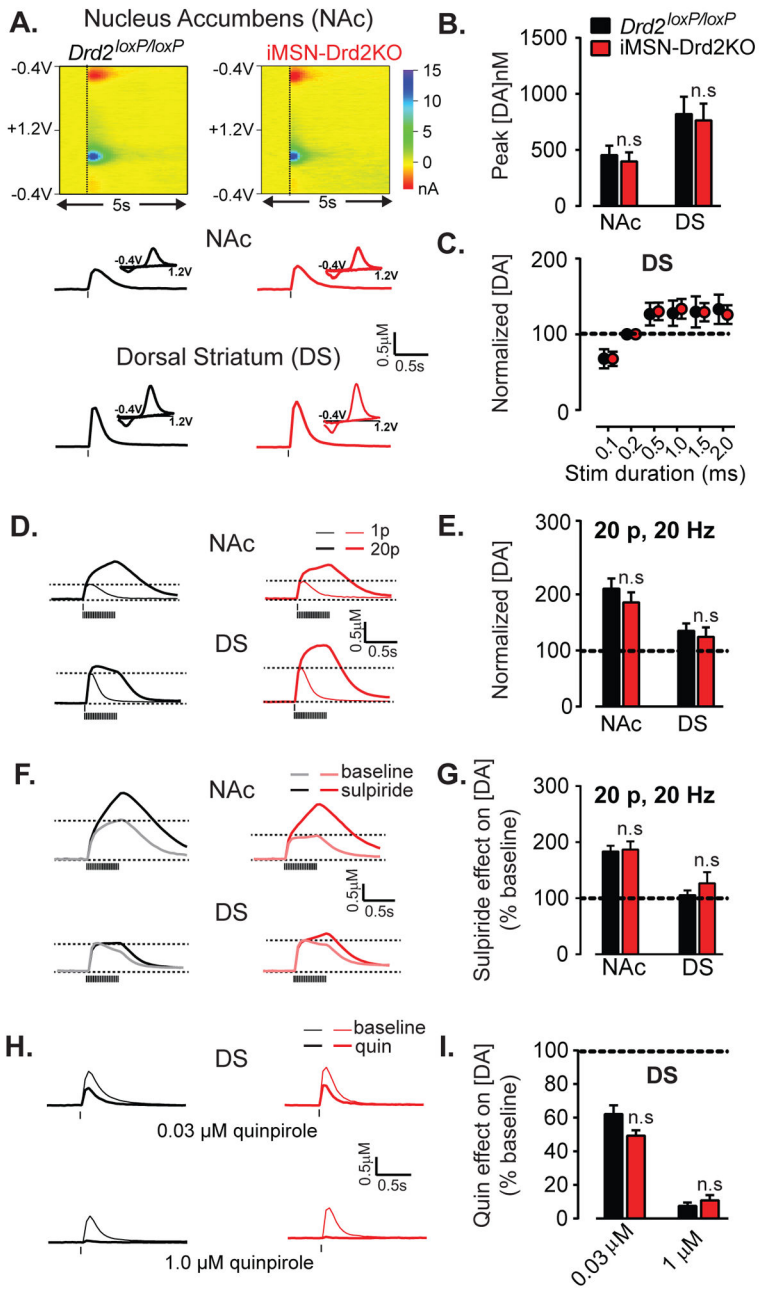

Figure 3. iMSN-Drd2KO mice show intact dopamine transmission

a) *Top*, Representative 3-D graphs showing recorded current (color scale) through the carbon fiber as a function of time (x-axis) and voltage applied (y-axis) recorded using fast scanning cyclic voltammetry in brain slices. *Bottom*, Representative traces of DA transients and current-voltage plots corresponding to the peak (*inset*) recorded in NAc and DS of *Drd2*$^{loxP/loxP}$ and iMSN-Drd2KO mice. **b**) Amplitude of DA concentration transients evoked by a single pulse stimulation, n = 7–14. **c**) Input-output curve of DA transient amplitude as a function of electrical pulse durations for the two genotypes. Data expressed as percent of peak evoked by 0.2 ms duration pulse in the DS, n = 5–9. **d,e**) Traces of DA transients

evoked by a single pulse (thin) and by a train of 20 pulses delivered at 20 Hz (thick) and plot of mean amplitude evoked by trains relative to single pulse in NAc and DS, n = 7–14. **f, g**) Traces of DA transients evoked by 20-pulse trains before (light) and after (dark) application of sulpiride (1 μM) and mean amplitude of DA transients in sulpiride normalized to baseline before sulpiride, n = 4–10. **h**) Example traces of DA transients evoked by single pulse stimulation before (light) and after (dark) application of quinpirole (0.03 μM; top) and (1 μM; bottom) in DS of both genotypes. **i**) Amplitude of DA transients after quinpirole (0.03 and 1 μM) relative to baseline, n= 4–9. n.s. = post-hoc tests, $p > 0.05$.

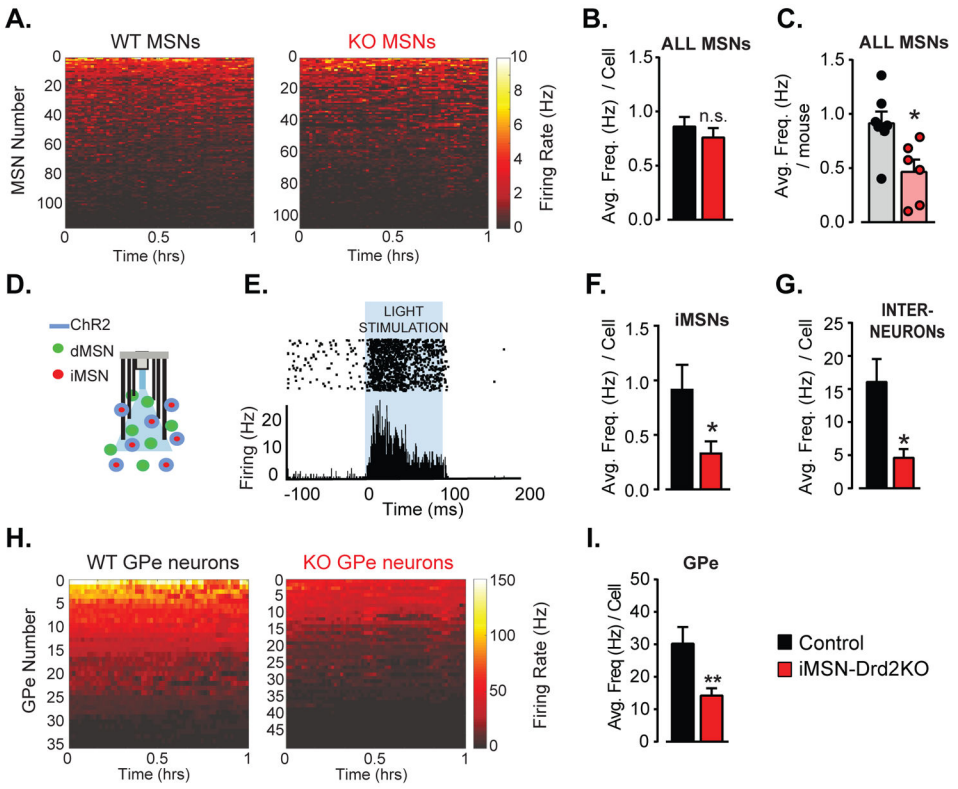

Figure 4. Low firing rate of MSNs and GPe neurons in freely moving mice with targeted deletion of D2Rs from iMSNs

a) Firing rate (Hz) of all MSNs recorded in the DS of freely moving control and iMSN-Drd2KO mice over a 1h-session is plotted in pseudo-color and displayed from high to low firing rate, n = 107–117 cells. **b**) Average firing rate per MSN in control and iMSN-Drd2KO during the 1h-session, n = 107–117 cells. **c**) Average MSN firing rate per animal in control and iMSN-Drd2KO during the 1h-session, n = 5–7 mice. **d**) Schematic of optogenetic tagging showing ChR2 expression in iMSNs and implanted micro-array with multi-electrode and fiber optic. **e**) Example recording of opto-tagged MSNs (putative iMSNs) showing increase in firing rate upon light stimulation. **f**) Average firing rate of opto-tagged iMSNs in *Adora2A-Cre*$^{+/-}$ control and iMSN-Drd2KO mice, n = 5–6 cells, 3 mice. **g**) Average firing rate of putative interneurons, n = 9–11 cells, 5–7 mice. **h**) Firing rate (Hz) of GPe neurons recorded in freely moving control and iMSN-Drd2KO mice over a 1h-session plotted in pseudo-color and displayed from low to high firing rate, n = 35–49 cells. **i**) Average firing rate of GPe neurons in control and iMSN-Drd2KO, n = 35–49 cells. *, ** t-tests, $p < 0.05$, 0.01 respectively.

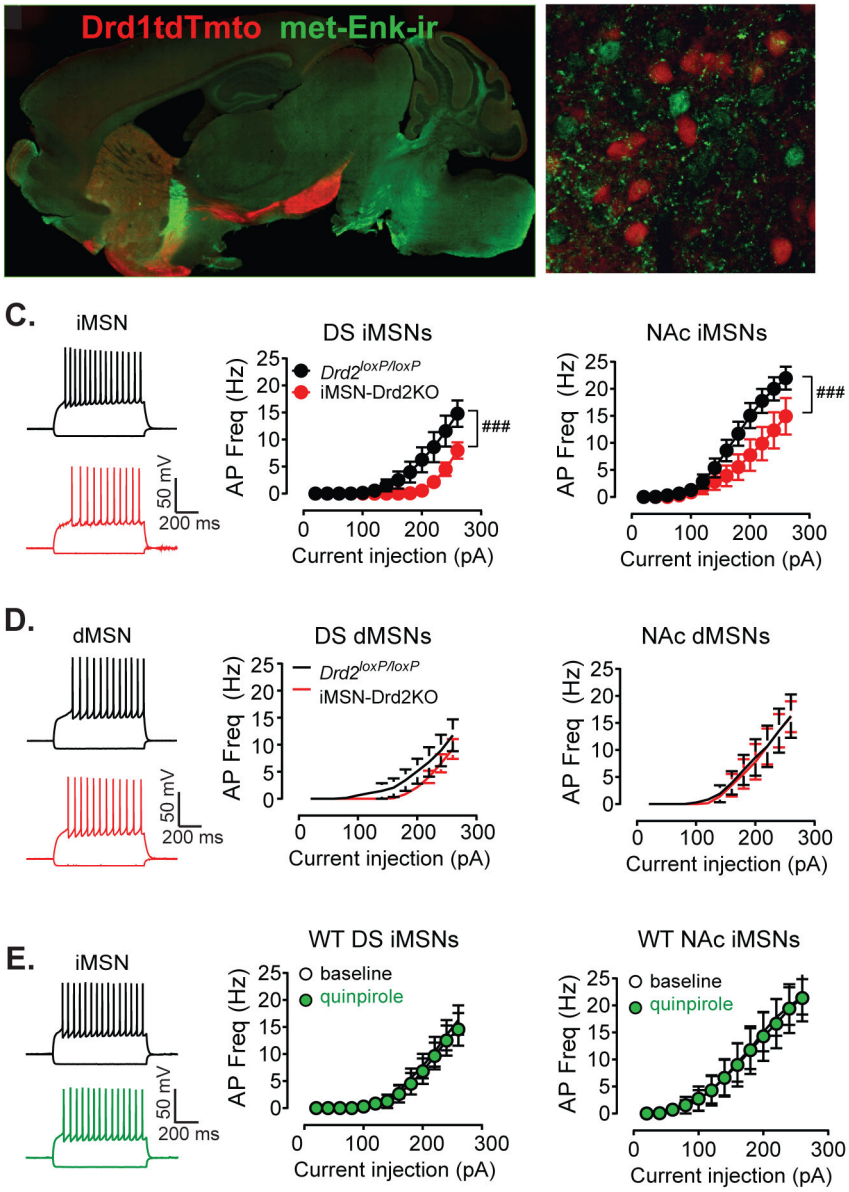

Figure 5. Reduced intrinsic excitability of iMSNs

a,b) Low- and high-power fluorescent images of the striatum of *Drd1tdTmto;D2*$^{loxP/loxP}$ showing pattern of expression and segregation of Tdtmto-positive D1R-containing putative dMSNs (red) and met-enkephalin-positive putative D2R-containing iMSNs (green). **c,d**) Example traces of membrane potential recordings following hyperpolarizing (−160 pA) and depolarizing current steps (260 pA) in nonlabeled putative iMSNs and red-fluorescence-positive putative dMSNs in *Drd2*$^{loxP/loxP}$ and iMSN-Drd2KO mice crossed in *Drd1tdTmto* background. **c,d**) Input-output curve for AP frequency in iMSNs (c) and dMSNs (d) following current steps of increasing amplitudes recorded in the presence of synaptic blockers in the DS and NAc, n = 6–14 and 5–9. ###, current x genotype interaction, $p < 0.001$. **e**) Example traces and mean data showing the effect of quinpirole (1 μM) on AP firing in iMSNs recorded from WT *Drd1-tdTomato* mice in the DS and NAc, n = 6–7.

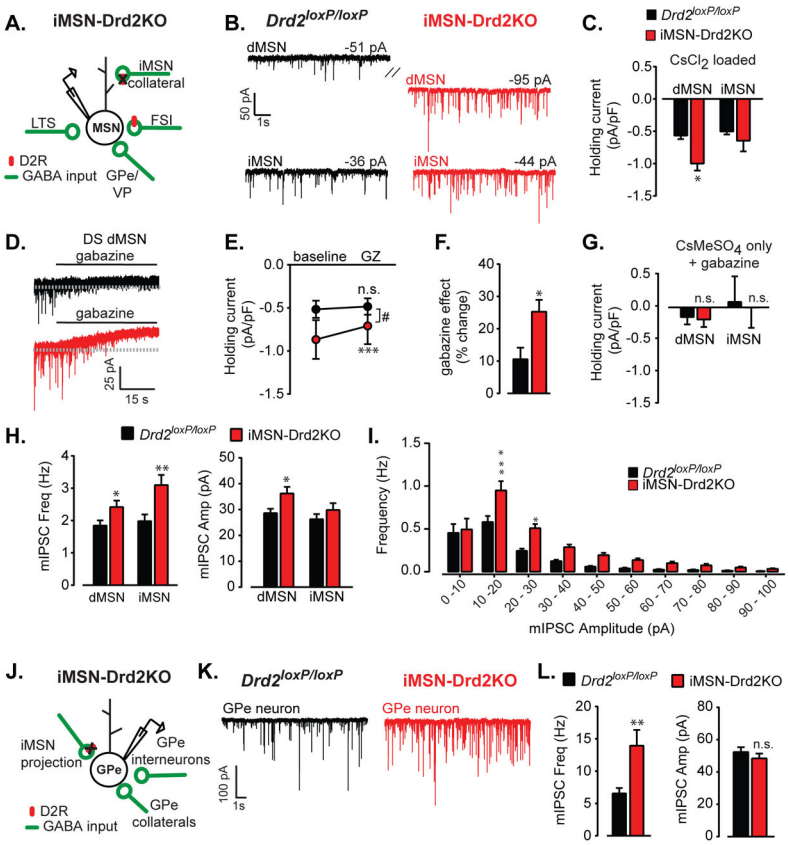

Figure 6. Enhanced GABAergic tone following deletion of D2Rs from iMSNs

a) Schematic depicting the main sources of synaptic GABAergic inputs (green) onto MSNs. Red oval represents D2Rs, which are lacking in iMSN-Drd2KO mice. b) Example traces of mIPSCs recorded from red-positive dMSNs and red-negative iMSNs in *Drd1tdTmto;Drd2*$^{loxP/loxP}$ and *Drd1tdTmto;*iMSN-Drd2KO mice. Hatch mark indicates a significant difference in holding current recorded from dMSNs in control and KO mice. **c**) Holding current density in dMSNs and iMSNs recorded from the striatum (DS and NAc combined) using 50/50 $CsMeSO_3$/$CsCl_2$ internal, n = 14–25. **d, e**) Example traces (d) and collapsed holding current density prior to and following bath application of gabazine (10 μM) recorded from dMSNs in the DS of *Drd2*$^{loxP/loxP}$ and iMSN-Drd2KO mice, n = 8–9. **f**) Percentage change in holding current density following gabazine application in each genotype, n = 8–9. **g**) Holding current density in dMSNs and iMSNs recorded from the DS using 100% $CsMeSO_3$ internal and in the presence of gabazine, n = 12–16. **h**) mIPSC frequency and amplitude in dMSNs and iMSNs recorded from the striatum (DS and NAc combined) of both genotypes, n = 14–25. **i**) Frequency histogram of mIPSC amplitude for both genotypes (combined NAc and DS). **j**) Schematic depicting the main sources of synaptic GABAergic inputs (green) onto GPe neurons. **k**) Example traces of mIPSCs recorded from GPe neurons. **l**) mIPSC frequency and amplitude recorded in GPe neurons of both genotypes, n = 17–19. *, **, *** t-tests or post-hoc tests, $p < 0.05, 0.01, 0.001$ respectively.

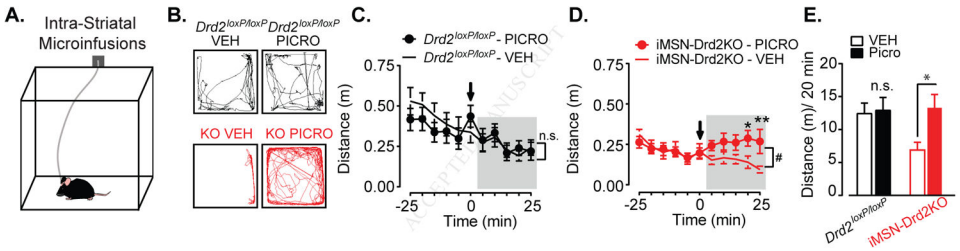

Figure 7. Enhanced GABA tone in the striatum is a key driver of locomotor deficit

a) Schematic of behavioral paradigm depicting mouse tethered to the infusion line. **b**) Representative track traces for *Drd2*$^{loxP/loxP}$ (black) and iMSN-Drd2KO (red) mice following vehicle (ACSF; left) or picrotoxin (100 μM; right) infusion. **c**) Timecourse of locomotor activity in *Drd2*$^{loxP/loxP}$ mice before and after infusion of vehicle (ACSF; open circle) or picrotoxin (closed circles), n = 15. **d**) Timecourse of locomotor activity in iMSN-Drd2KO mice before and after infusion of vehicle (ACSF; open circle) or picrotoxin (closed circles), n = 16. #, time x drug interaction, $p < 0.05$, *,** post-hoc tests, $ps < 0.05$ and 0.01 respectively. **e**) Collapsed post-infusion locomotor activity (cumulative activity over shaded period) for *Drd2*$^{loxP/loxP}$ and iMSN-Drd2KO mice infused with either vehicle or picrotoxin, n = 15–16, * post-hoc test, $p < 0.05$.

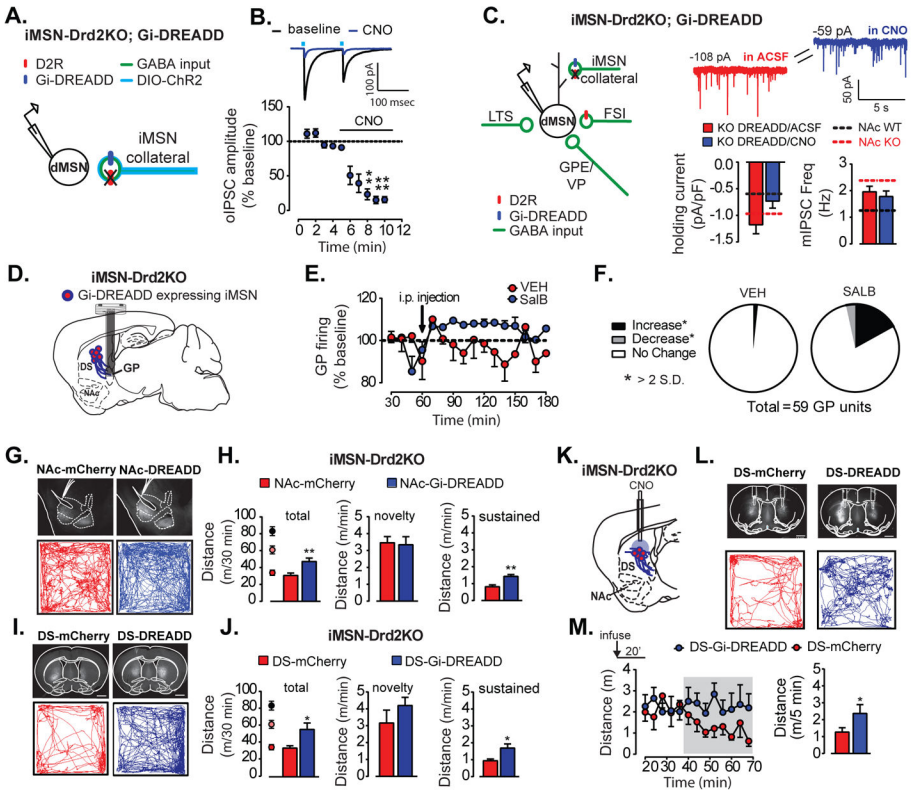

Figure 8. Activation of Gi-DREADD in iMSNs reduces GABAergic tone and partially rescues locomotor deficit

All graphs and data in this figure correspond to iMSN-Drd2KO mice **a**) Schematic of experimental configuration showing optogenetic stimulation of iMSN axon collaterals expressing hM4Di and recordings from neighboring putative dMSNs. **b**) *Top,* Averaged oIPSCs traces recorded from dMSNs before and after CNO application and *Bottom*, Timecourse of CNO effect on oIPSC amplitude. ** post-hoc tests, $p = 0.01$. **c**) *Left,* Diagram showing targeted expression of hM4Di-mCherry (blue oval) to iMSNs. *Right,* Example traces of mIPSCs and holding current recorded from NAc dMSNs with selective expression hM4Di-mCherry before and after CNO application. Bar graphs show mean density of holding current and mIPSC frequency before and after CNO. Dashed lines indicate mean measurements for naïve $Drd2^{loxP/loxP}$ (black) and iMSN-Drd2KO (red) mice. * t-test, $p < 0.05$. **d**) Schematic of experimental configuration in which the Gi-DREADD KOR is expressed in iMSNs of iMSN-Drd2KO mice and microarrays are implanted in GPe. **e**) *In vivo* firing rate of GPe neurons before and after vehicle (DMSO) or SalB administration (*i.p.*), displayed as percent of pre-injection rate.. **f**) Proportion of single units that increased or decreased (>2 SD from baseline) or showed no change in the firing rate in response to systemic administration of vehicle or SALB. **g, i**) *Top*, Representative images of iMSN-Drd2KO brain sections showing localized expression of hM4di-mCherry or control mCherry in NAc (g) or DS (i) (Scale bar = 1 mm). *Bottom*, Representative track traces of locomotion in novel open-field over 30 min after CNO (1 mg/kg, *i.p.*) in iMSN-Drd2KO mice expressing mCherry and hM4Di-mCherry in NAc (g) or DS (i). **h,j**) Total distance traveled over 30 min (left) and average speed (m/min) for the first minute (novelty phase,

middle) and the last 20 min (sustain phase, right) for iMSN-Drd2KO mice expressing mCherry and hM4Di-mCherry in the NA(h) or DS (j). Black, pink and red circles represent mean ± SEMs for the three naïve genotypes. *, ** t-tests, *ps* < 0.05 or 0.01 respectively. **k**) Schematic of experimental configuration in which Gi-DREADD hM4Di or control mCherry are expressed in iMSNs in the DS of iMSN-Drd2KO mice and local infusion of CNO is performed into DS. **l**) *Top*, Coronal brain sections from iMSN-Drd2KO showing bilateral DS cannulations and localized expression of hM4di-mCherry or control mCherry in the DS (Scale bar = 1 mm). *Bottom*, Representative track traces of locomotion in open-field over the last 30 min following CNO microinfusion in the DS of iMSN-Drd2KO mice expressing mCherry and hM4Di-mCherry. **m**) *Right*, Timecourse of locomotor activity in the last 50 minutes post-CNO infusion for mCherry and hM4Di-mCherry infected animals. *Left,* Distance traveled per 5 min during the last 30 minutes (shades area of timecourse). * t-test, $p < 0.05$.